VNU Journal of Science: Mathematics - Physics

Journal homepage: https://js.vnu.edu.vn/MaP

Original Article

Structural and Mechanical Properties of Cubic Silicon Nitride: A Molecular Dynamics Study

Nguyen Thi Thao[1], Nguyen Thi Thanh Ha[2], Le Van Vinh[3,*]

[1]*Hanoi National University of Education, 136 Xuan Thuy, Cau Giay, Hanoi, Viet Nam*

[2]*School of Engineering Physics, Hanoi University of Science and Technology, 1 Dai Co Viet, Hai Ba Trung, Hanoi, Viet Nam*

[3]*Phenikaa University, Nguyen Van Trac, Ha Dong, Hanoi, Vietnam*

Received 12 January 2022
Revised 16 March 2022; Accepted 17 March 2022

Abstract: The molecular dynamics simulations have been used to study the microstructure as well as mechanical behavior of cubic silicon nitride (c-Si_3N_4) under the extended deformation. The silicon nitride sample was simulated under the cooling process and high pressure. At T=300 K, dominant nitrogen (N) atoms arrange into fcc lattice, and the rest of N atoms have hexagonal close-packed (hcp) and disordered structures. The hcp and disordered N atoms gather into the narrow bands. The phonon spectra of this sample are calculated and discussed. In this work we also present a molecular dynamics prediction for the elastic moduli in strained cubic silicon nitride as functions of the volumetric strain. Young's modulus and Poisson's ratio are also calculated for the c-Si_3N_4.

Keywords: Molecular dynamics, Si_3N_4, Cubic, Mechanical, Deformation.

1. Introduction

Silicon nitride (Si_3N_4) is widely used in technological applications due to its very high mechanical strength, high thermal and chemical stability, and useful semiconducting properties [1]. Beside α- and β-Si_3N_4 phases at the normal condition [2], third phase of Si_3N_4 crystals has been synthesized third phase at P ≥15 GPa and T ≥ 2000 K, in which Si_3N_4 crystallizes into a cubic spinel-type structure called γ-Si_3N_4 [3]. The γ-Si_3N_4 has excellent mechanical properties with the hardness up to 43 GPa [4, 5]. By shock wave compression, γ-Si_3N_4 has been also prepared from α- and β-Si_3N_4. The Si_3N_4 powders were

* Corresponding author.
E-mail address: vinh.levan@phenikaa-uni.edu.vn

https//doi.org/10.25073/2588-1124/vnumap.4699

quenched upon the shock pressure of 12 to 115 GPa, in which 80% of the γ-Si_3N_4 recovered at P=54 GPa and T=2400 K with grain sizes 10-50 nm [6]. The γ-Si_3N_4 obtained to 80% percent at the shock pressure of 45 GPa and T=4000 K by using the mixtures of α-Si_3N_4 and copper powders as initial materials [7]. In fact, the β-γ phase transition pressures are difficult to determine in a wide temperature range [8]. Moreover, the grain size of the γ-Si_3N_4 decreases with an increase in synthesis pressure and thus the higher pressure is favorable for eliminating pores and defects along the grain boundaries, leading to enhance the mechanical properties with improvement in the hardness [4]. Based on the optimization of the geometric structure, The first-principles calculations have shed light on why cubic (c-) Si_3N_4 has the spinel structure under the high pressure and high temperature [9, 10]. The mechanical behaviors of c-Si_3N_4 crystals have been investigated by applied the deformation. The stress-strain curves of the c-Si_3N_4 were obtained by applied tensile and shear stress, in which the ideal tensile and shear strength were determined to be 45 and 49 GPa, respectively [11]. However, these first-principles calculations have been carried out on the perfect structure of the γ-Si_3N_4 while the experiments showed that the structure of the γ-Si_3N_4 contains grain boundaries and defects [4, 12]. At the atomistic scale, molecular dynamics (MD) simulations represent a powerful complement to experimental techniques with providing mechanistic insight into experimentally observed processes [13]. Recently, the mechanical properties of β-Si_3N_4 nanoporous membranes have been studied by MD simulations under the tensile deformation, suggesting that the proper introduction of the pores in nanoporous membranes leads to the transition from brittle to ductile transition in the failure mechanism [14]. Thus, in this work, we used the MD simulations to study the microstructure and mechanical behavior of the c-Si_3N_4. The c-Si_3N_4 sample was obtained by the quenching process under high pressures. The microstructure of the c-Si_3N_4 sample is characterized by the radial distribution function (RDF), fractions of SiN_x structural units, bond angle distribution (BAD), common neighbor analysis (CNA), and atomic visualization. The extended deformation was applied to the c-Si_3N_4 sample to investigate the mechanical properties of the sample.

2. Computational Procedures

In the MD simulation we used the two-body potential which can be found in elsewhere [15]. The pair potential is described in two terms only, including the attractive Morse-type for Si-N pair, the screened Coulomb repulsion for Si-Si and N-N pairs, and the additional dispersion term for N-N interactions. This potential has been chosen because it is computationally efficient, yields models with moderately low coordination defects and reasonable values for the enthalpy of formation [16]. The MD simulations were executed at a constant pressure (the ensemble NPT) with the Verlet algorithm and a time step of 1 fs. The periodic boundary condition was used to the simulation box. The Berendsen thermostat and barostat were applied during the simulation process to control the temperature and pressure of the systems [17].

The Si_3N_4 sample contains 4500 Si and 6000 N atoms. The coordinates of these atoms were generated randomly in the simulation box with the size of 55 Å × 55 Å × 55 Å. The random generation ensures that the distance between neighboring atoms is always higher than 1.0 Å. This initial configuration was used as the input for the MD simulation. This Si_3N_4 sample was heated at T = 5000 K and the P = 0 GPa for 100 ps. Then, the sample was cooled down to T = 300 K with the cooling rate of 10^{-13} K/s and P = 45 GPa.

To calculate the mechanical properties, the sample was deformed by the uniform expansion of magnitude in each of the x, y and z directions. The energy – volume curve was obtained by the extending direction. The bulk modulus can be calculated as [18]:

$$B(V) = -VP'(V) = VE''(V), \tag{1}$$

where V is the volume of unit cell, E(V) is the corresponding energy per unit cell, and P(V) is the pressure. The second derivative $E''(V)$ must be approximated because the calculations provide only a set of $E(V_i)$ for a limited number of V_i. The E(V) is calculated to the form proposed by Birch [18]:

$$E(V) = E_0 + \frac{9}{8}B_0V_0\left[\left(\frac{V_0}{V}\right)^{2/3} - 1\right]^2 + \frac{9}{16}B_0V_0(B_0' - 4)\left[\left(\frac{V_0}{V}\right)^{2/3} - 1\right]^3 + \sum_{n=4}^{N}\gamma_n\left[\left(\frac{V_0}{V}\right)^{2/3} - 1\right]^n, \tag{2}$$

where E_0, B_0, V_0 and B_0' are the equilibrium energy, volume, bulk modulus, and pressure derivative of the bulk modulus, respectively, and while N is the fitting order. Eq. (2) is a special case of the general expression:

$$E(V) = \sum_{n=0}^{N}\alpha_n V^{-2n/3}, \tag{3}$$

where α_n are the fitting parameters. This Birch fit was used to obtain the bulk modulus B and the shear modulus G. Thus, Young's modulus can be estimated as:

$$E = \frac{9BG}{(3B+G)}, \tag{4}$$

and the Poisson's ratio can be calculated as:

$$\sigma = \frac{(3B-2G)}{2(3B+G)} \tag{5}$$

3. Results and Discussion

The local structure of Si_3N_4 sample has been analyzed via the pair RDFs as presented in Figue 1. The pair functions, $g_{Si-N}(r)$, $g_{Si-Si}(r)$ and $g_{N-N}(r)$, show many clear and sharp peaks, indicating the ordered structure of Si_3N_4. The first, second and third peaks of the $g_{Si-N}(r)$ locate at 1.83 ± 0.01, 3.24 ± 0.01 and 4.17 ± 0.01 Å, respectively. Based on this $g_{Si-N}(r)$, the first minimum after the first peak is determined as 2.23 ± 0.01 Å and this value is used to calculate the SiN_x units. Fraction of SiN_4, SiN_5 and SiN_6 units is calculated as 10.16, 8.80 and 81.04 %, respectively. Obviously, network structure of Si_3N_4 consists of dominant SiN_6 units and significant SiN_4 and SiN_5 units. The first, second and third peaks of the $g_{N-N}(r)$ locate at 2.59 ± 0.01, 3.67 ± 0.01 and 4.57 ± 0.01 Å, respectively, while those of the $g_{Si-Si}(r)$ locate at 2.67 ± 0.01, 3.08 ± 0.01 and 3.70 ± 0.01 Å, respectively. Here we note that, in the $g_{N-N}(r)$, the distance of the second peak is approximately equal to the distance of the first peak multiplied by $\sqrt{2}$, indicating that the sublattice of N atoms can be arranged in the face-centered cubic (fcc) structure. To elucidate the structure of Si_3N_4, the CNA was used to determine the crystalline atoms [19]. Here we found that 67.35 % of N atoms arrange in the fcc structure while 5.65 % of those arrange in the face-centered cubic (hcp) structure and 27 % of those are in the disordered (d-) structure. The cross-sectional structures of Si_3N_4 with the fcc, hcp and d- structures are showed in Figure 2. As observed in Figure 2, the fcc N atoms link together to create fcc N structure which connects to Si atoms which are distributed only in dominant SiN_6 units and significant SiN_4 units. The crystalline structure of c-Si_3N_4 is isostructural with the mineral $MgAl_2O_4$ [20] which has a fcc lattice with space group $Fd\bar{3}m$. The ideal spinel structure consists of a fcc sublattice of N atoms with the Si ions occupying both one eighth of the interstitial tetrahedral sites and one half of the octahedral sites [21]. Thus, this c-Si_3N_4 is formed with the fcc N sublattice linked to significant SiN_4 units and dominant SiN_6 units. It is noted that the simulated distances of Si-N, Si-Si and N-N bond lengths are close to the experimental data of γ-Si_3N_4 [22] in which the distances of Si-N_{tet}, Si-N_{oct}, Si-Si and N-N bond lengths are 1.7849, 1.8718, 2.7343 and 2.5539 Å, respectively. Meanwhile, hcp and d- N atoms gather to form narrow bands that surround the fcc N sublattice. These hcp and d- N atoms connect to Si atoms which are distributed in SiN_6, SiN_5 and SiN_4 units. We calculated the average potential energy (APE) of these fcc, hcp and d- N atoms in which the APE of fcc N atoms is -8.095 eV/atom while that of hcp and d- N atoms are -7.105 and -6.929 eV/atom, respectively. Thus, these hcp and d- N atoms are classified as the stacking faults and defects in the fcc N lattice, respectively. Furthermore, almost Si atoms from SiN_5 units connect to hcp and d- N atoms. These SiN_5 units are considered as the most common defects [23]. We also examined the geometries of SiN_4 and SiN_6 units in the Si_3N_4 sample. Figure 3 shows the BADs of SiN_4 and SiN_6 units. For both of SiN_4 and SiN_6 units, the peak of the BAD in fcc structure are higher and sharper than that of the BAD in hcp and d- structures, indicating that SiN_4 and SiN_6 units in hcp and d- structures are more distorted than those in the fcc structure. Consequently, the narrow bands including hcp and d- N structures are considered as the stacking faults and defects in the fcc N structure of c-Si_3N_4. The narrow bands of hcp and d- N structures are observed as the grain boundaries which are observed by STEM images [12]. This suggests that MD simulations can aid to understand more insight of structural grain boundaries at the atomic level.

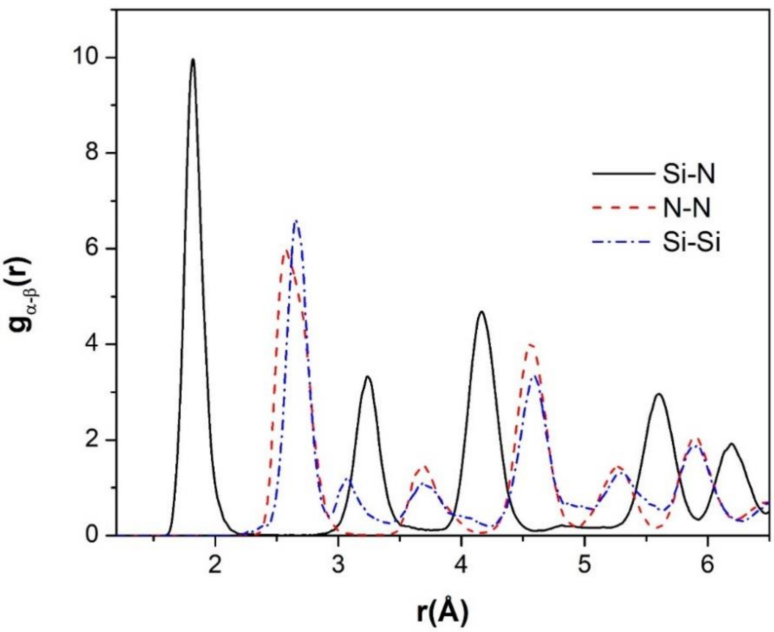

Figure 1. The pair RDFs of Si_3N_4 at T= 300 K.

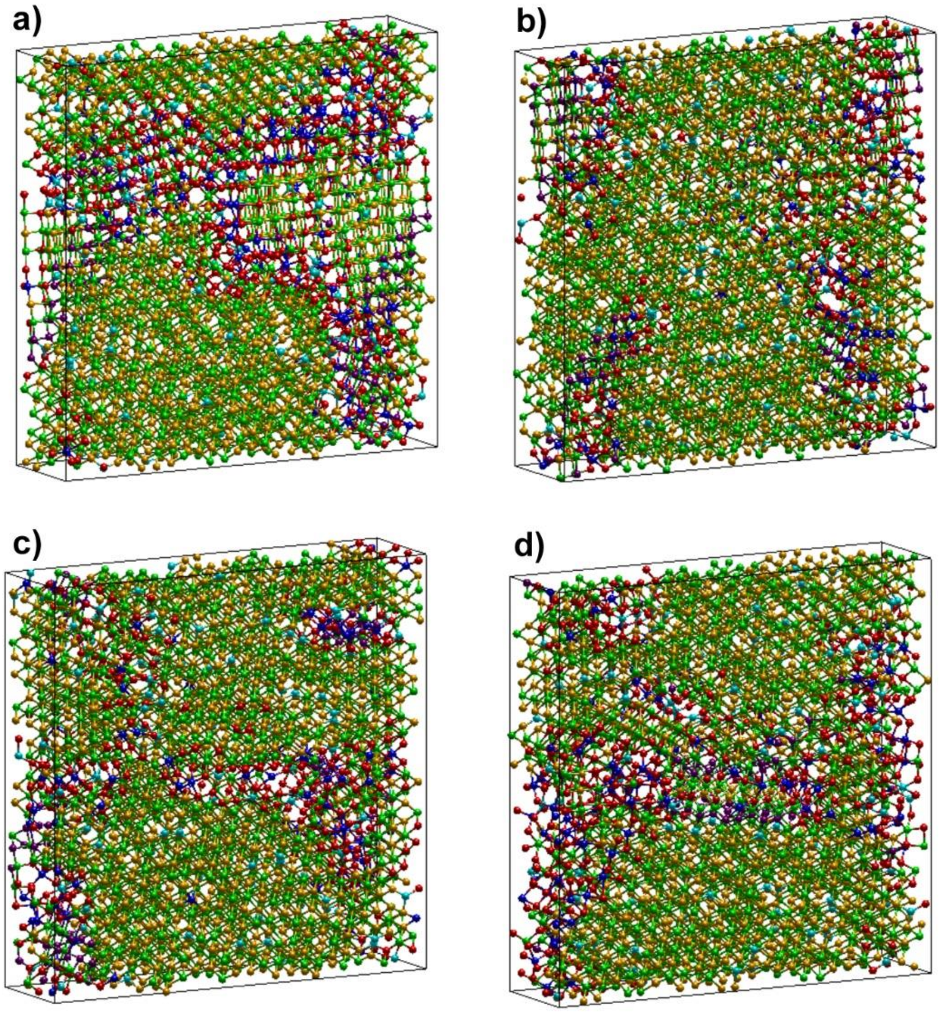

Figure 2. Cross-sectional Si_3N_4 sample ($L_x \times L_y \times L_z$) at the position: a) $L_x/4$, b) $L_x/2$, c) $3L_x/4$ and d) L_x (yellow color: fcc N atom, violet color: hcp N atom, red color: a- N atom, cian color: Si atom from SiN_4 unit, blue color: Si atom from SiN_5 unit and green color: Si atom from SiN_6 unit).

The phonon spectra P(ω) of this c-Si_3N_4 are calculated by using the fast Fourier transform on the velocity autocorrelation function [24]:

$$P(\omega) = \frac{1}{\sqrt{2\pi}} \int_0^{\infty} \left\langle \sum_{i=1}^{N} v_i(t) v_i(0) \right\rangle e^{i\omega t} d\omega , \tag{6}$$

where $v_i(t)$ and ω are the velocity and angular frequency of the atom "i" at time t, respectively. The ensemble average here is substituted by time averaging, which is performed over 30 ps after the realization of the equilibrium state. Figure 4 shows the calculated partial and total phonon density of states (PDOS) of c-Si_3N_4 sample. The total PDOS spans up to about 1145 cm^{-1}, which is about 2.3% and 10% greater than the maximum frequencies (1119 and 1030 cm^{-1}) obtained by Marian et al. [15] and by Fang et al. [21], respectively. We note that the γ-Si_3N_4, obtained by ab initio simulations [21], does not consist of SiN_5 units in the network structure. Different vibration contributions from three different Si atoms are recognizable as presented in Figure 4. The low energy vibrations (<550 cm^{-1}) originate mainly from Si atoms. The N atoms are involved in the vibrational modes over the high energy range (>670 cm^{-1}).

In applying the MD simulations to the moduli calculation, the sample was extended uniformly in the x, y and z directions at T = 300 K in NPT ensemble. The energy and volume of the system were determined at the same time. The energy-volume curve is showed in Figure 5. Based on this curve, the system energy as a function of the volume (V$^{-2/3}$) can be estimated by a function using the equation (3) with the following coefficients obtained through curve fitting:

$$\begin{aligned} \alpha_0 &= -83 \\ \alpha_1 &= 4786 \\ \alpha_2 &= \text{-}103950 \\ \alpha_3 &= 1000910 \\ \alpha_4 &= \text{-}3605650 \end{aligned} \tag{7}$$

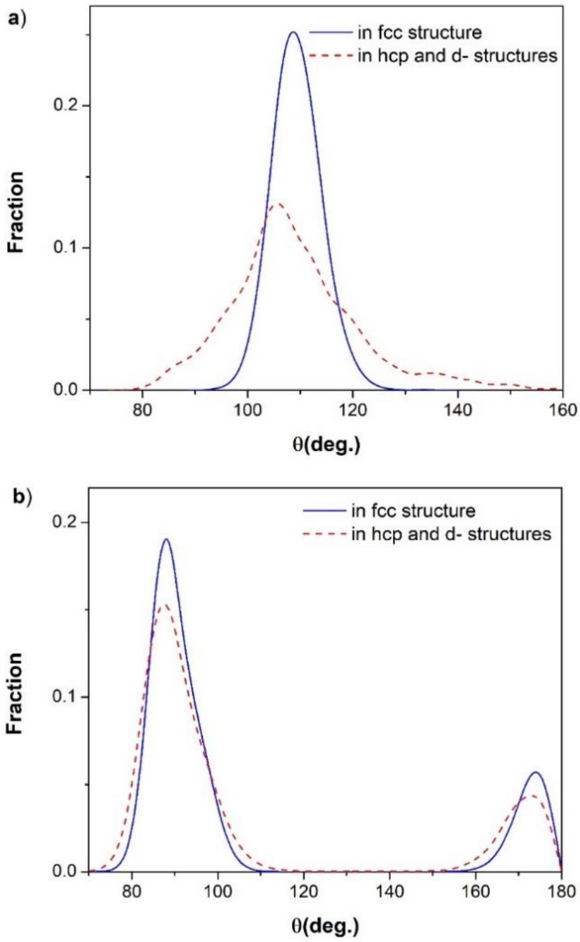

Figure 3. The bond angle distribution in: a) SiN_4 units and b) SiN_6 units.

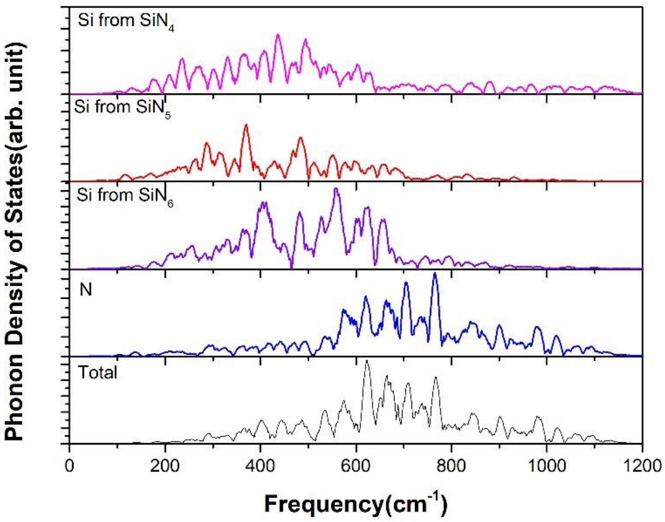

Figure 4. Partial and total PDOS for c-Si_3N_4 calculated from this MD simulations.

Now, we used these coefficients in Eq. (7) to calculate the bulk modulus in Eq. (1), B=308 GPa and this value is good agreement with experimental data [5, 12] and other calculations [11].

For a cubic crystal, the elastic moduli can be divided into two classes, the bulk modulus $B=(C_{11}+2C_{12})/3$, and the two shear moduli, C_{11}-C_{12} and C_{44} [25]. The shear moduli can be estimated the derivative of the energy as a function of a lattice strain [26]. The total energy can be expressed in powers of the strain [25],

$$E(\delta) = E(-\delta) = E(0) + (C_{11} - C_{12})V_0\delta^2 + O[\delta^4], \tag{8}$$

and

$$E(\delta) = E(-\delta) = E(0) + \frac{1}{2}C_{44}V_0\delta^2 + O[\delta^4], \tag{9}$$

where E(0) is the energy of unstrained lattice at the volume V_0, and the dilation δ is given by,

$$\delta = \frac{V - V_0}{V_0}. \tag{10}$$

As observed in Figure 2, since the c-Si_3N_4 sample is not true isotropic materials, bound on G can be determined by Hashin and Shtrikman [27],

$$G_1 = G_1^* + \frac{3(G_2^* - G_1^*)}{5 - 4\beta_1(G_2^* - G_1^*)}, \tag{11}$$

and

$$G_2 = G_2^* + \frac{2(G_1^* - G_2^*)}{5 - 6\beta_2(G_1^* - G_2^*)}, \tag{12}$$

where

$$G_1^* = \frac{(C_{11} - C_{12})}{2}, \; G_2^* = C_{44} \tag{13}$$

and

$$\beta_1 = -\frac{3(B + 2G_1^*)}{5G_1^*(3B + 4G_1^*)}, \; \beta_2 = -\frac{3(B + 2G_2^*)}{5G_2^*(3B + 4G_2^*)} \tag{14}$$

The Hashin bound G_H is designated as the larger of G_1 and G_2, while the Shtrikman bound G_S is the smaller. Thus, G can be calculated as,

$$G = \frac{G_H + G_S}{2} \tag{15}$$

From the c-Si_3N_4 sample, G is estimated as 186 GPa. In the experiments, the value of the G is determined as 148 GPa [5] and 247.5 GPa [12] because of the anisotropy of this c-Si_3N_4 sample. Thus, the value of 186 GPa from our calculations is reasonable. Here the value of Young's modulus is determined as 464 GPa and the value of Poisson's ratio is estimated as 0.248. We note that the size effect of sample on the microstructure and mechanical property is not investigated in this work.

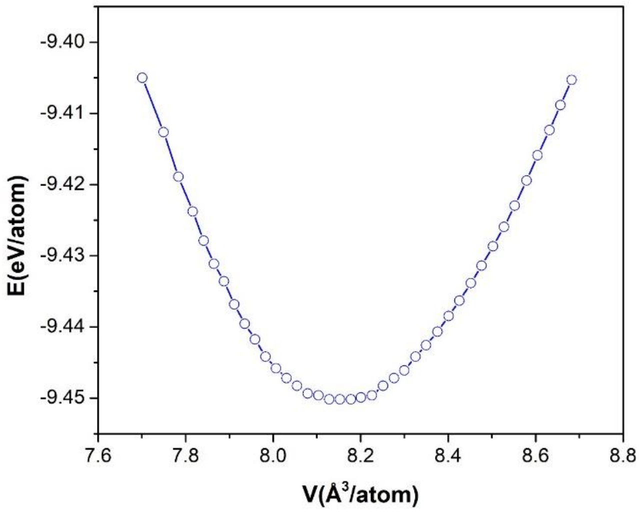

Figure 5. The total energy versus the volume system at T=300 K.

4. Conclusion

c-Si_3N_4 sample was simulated by the MD simulations under the cooling process and high pressure of 45 GPa. The c-Si_3N_4 contains dominant fcc N atoms linked to the Si atoms which are distributed in both significant SiN_4 and dominant SiN_6 units. The hcp and d- N atoms gather into the band, in which Si atoms are distributed in dominant SiN_6 units, significant SiN_5, and significant SiN_4 units. The bands of hcp and d- N atoms are considered such as the grain boundaries in the c-Si_3N_4. The PDOS has a cut-off energy of 1145 cm^{-1} with the contributions from N atoms in the high energy range (550 – 1145 cm^{-1}), while the contributions from Si atoms are predominantly over the lower energy range. The extended deformation was carried out on the c-Si_3N_4 sample. The MD-simulated value of bulk modulus well consists with those measured experimentally and calculated from the first-principles calculations. The value of the shear modulus, G=186 GPa, is reasonable due to the anisotropy of the c-Si_3N_4. Young's modulus and Poisson's are also determined based on these bulk and shear moduli.

Acknowledgments

This research is funded by Vietnam National Foundation for Science and Technology Development (NAFOSTED) under grant number 103.05-2019.364.

References

[1] E. S. Gonzalez, P. Miranda, F. Guiberteau, A. Pajares, Effect of Temperature on The Pre-creep Mechanical Properties of Silicon Nitride, Journal of the European Ceramic Society, Vol. 29, No. 12, 2009, pp. 2635-2641, https://doi.org/10.1016/j.jeurceramsoc.2009.03.011.

[2] K. Chen, Z. Huang, Y. Liu, M. Fang, J. Huang, Y. Xu, Synthesis of β-Si_3N_4 Powder from Quartz via Carbothermal Reduction Nitridation, Powder Technology, Vol. 235, 2013, pp. 728-734, https://doi.org/10.1016/j.powtec.2012.11.036.

[3] A. Zerr, G. Miehe, G. Serghiou, M. Schwarz, E. Kroke, R. Riedel, H. Fueb, P. Kroll, R. Boehler, Synthesis of Cubic Silicon Nitride, Nature, Vol. 400, 1999, pp. 340-342, https://doi.org/10.1038/22493.

[4] S. Ma, Y. Zhao, R. Tang, B. Yang, Q. Tao, Y. Li, J. Cheng, Y. Wang, T. Cui, P. Zhu, Transparent β-Si_3N_4 and γ-Si_3N_4 Compacts Synthesized with Mixed-size Precursor under High Pressure and High Temperature, Applied Physics Letters, Vol. 119, No. 17, 2021, pp. 171904, https://doi.org/10.1063/5.0070380.

[5] A. Zerr, M. Kempf, M. Schwarz, E. Kroke, M. Goken, R. Riedel, Elastic Moduli and Hardness of Cubic Silicon Nitride, Journal of the American Ceramic Society, Vol. 85, No. 1, 2002, pp. 86-90, https://doi.org/10.1111/j.1151-2916.2002.tb00044.x.

[6] T. Sekine, H. He, T. Kobayashi, M. Zhang, F. Xu, Shock-Induced Transformation of β-Si_3N_4 to A High-Pressure Cubic-Spinel Phase, Applied Physics Letters, Vol. 76, No. 25, 2000, pp. 3706-3708, https://doi.org/10.1063/1.126756.

[7] H. Yao, Q. Xu, J. Tang, Synthesis and Stability of Cubic Silicon Nitride, Advanced Materials Research, Vols. 79-82, 2009, pp. 1467-1470, https://doi.org/10.4028/www.scientific.net/AMR.79-82.1467.

[8] N. Nishiyama, J. Langer, T. Sakai, Y. Kojima, A. Holzheid, N. A. Gaida, E. Kulik, N. Hirao, S. I. Kawaguchi, T. Irifune, Y. Ohishi, Phase Relations in Silicon and Germanium Nitrides up to 98 GPa and 2400 °C, Journal of the American Ceramic Society, Vol. 102, No. 4, 2019, pp. 2195-2202, https://doi.org/10.1111/jace.16063.

[9] J. Z. Jiang, H. Lindelov, L. Gerward, K. Stahl, J. M. Recio, P. M. Sanchez, S. Carlson, M. Mezouar, E. Dooryhee, A. Fitch, D.J. Frost, Compressibility and Thermal Expansion of Cubic Silicon Nitride, Physical Review B, Vol. 65, 2002, pp. 161202, https://doi.org/10.1103/PhysRevB.65.161202.

[10] B. Kiefer, S. R. Shieh, T. S. Duffy, T. Sekine, Strength, Elasticity, and Equation of State of The Nanocrystalline Cubic Silicon Nitride γ−Si_3N_4 to 68 GPa, Physical Review B, Vol. 72, 2005, pp. 014102, https://doi.org/10.1103/PhysRevB.72.014102.

[11] C. Kocer, N. Hirosaki, S. Ogata, *Ab Initio* Calculation of The Ideal Tensile and Shear Strength of Cubic Silicon Nitride, Physical Review B, Vol. 67, 2003, pp. 035210, https://doi.org/10.1103/PhysRevB.67.035210.

[12] N. Nishiyama, R. Ishikawa, H. Ohfuji, H. Marquardt, A. Kurnosov, T. Taniguchi, B. N. Kim, H. Yoshida, A. Masuno, J. Bednarcik, E. Kulik, Y. Ikuhara, F. Wakai, and T. Irifune, Transparent polycrystalline cubic silicon nitride, Scientific Reports, Vol. 7, 2017, pp. 44755, https://doi.org/10.1038/srep44755.

[13] P. H. Hunenberger, Thermostat Algorithms for Molecular Dynamics Simulations, In: Dr. Holm, C., Prof. Dr. Kremer, K. (eds) Advanced Computer Simulation. Advances in Polymer Science, vol 173. Springer, Berlin, Heidelberg, 2005, pp. 105-149, https://doi.org/10.1007/b99427.

[14] A. K. Shargh, G. R. Madejski, J. L. McGrath, N. Abdolrahim, Molecular Dynamics Simulations of Brittle to Ductile Transition in Failure Mechanism of Silicon Nitride Nanoporous Membranes, Materialstoday Communications, Vol. 25, 2020, pp. 101657, https://doi.org/10.1016/j.mtcomm.2020.101657.

[15] C. M. Marian, M. Gastreich, J. D. Gale, Empirical Two-Body Potential for Solid Silicon Nitride, Boron Nitride, and Borosilazane Modifications, Physical Review B, Vol. 62, 2000, pp. 3117-3124, https://doi.org/10.1103/PhysRevB.62.3117.

[16] A. Dasmahapatra, P. Kroll, Modeling Amorphous Silicon Nitride: A Comparative Study of Empirical Potentials, Computational Materials Science, Vol. 148, 2018, pp. 165-175, https://doi.org/10.1016/j.commatsci.2017.12.008.

[17] H. J. C. Berendsen, J. P. M. Postma, W. F. van Gunsteren, A. DiNola, J. R. Haak, Molecular Dynamics with Coupling to An External Bath, The Journal of Chemical Physics, Vol. 81, 1984, pp. 3684-3690, https://doi.org/10.1063/1.448118.

[18] F. Birch, Finite Strain Isotherm and Velocities for Single-Crystal and Polycrystalline NaCl at High Pressures and 300 °K, Journal of Geophysical Research, Vol. 83, 1978, pp. 1257-1268, https://doi.org/10.1029/JB083iB03p01257.

[19] D. Faken, H. Jonsson, Systematic Analysis of Local Atomic Structure Combined with 3D Computer Graphics Computational Materials Science, Vol. 2, 1994, pp. 279-286, https://doi.org/10.1016/0927-0256(94)90109-0.

[20] N. W. Wyckoff, Crystal Structures, Vol.2, Interscience Publishers, New York, 1962.

[21] C. M. Fang, G. A. de Wijs, H. T. Hintzen, G. de With, Phonon Spectrum and Thermal Properties of Cubic Si_3N_4 from First-Principles Calculations, Journal of Applied Physics, Vol. 93, 2003, pp. 5175-5180, https://doi.org/10.1063/1.1566473.

[22] J. Z. Jiang, K. Stahl, R. W. Berg, D. J. Frost, T. J. Zhou, P. X. Shi, Structural Characterization of Cubic Silicon Nitride, Europhysics Letters, Vol. 51, No. 1, 2000, pp. 62-67, https://doi.org/10.1209/epl/i2000-00337-8.

[23] R. P. Vedula, N. L. Anderson, A. Strachan, Effect of Topological Disorder on Structural, Mechanical, and Electronic Properties of Amorphous Silicon Nitride: An Atomistic Study, Physical Review B, Vol. 85, 2012, pp. 205209, https://doi.org/10.1103/PhysRevB.85.205209.

[24] B. Liu, C. D. Reddy, J. Jiang, H. Zhu, J. A. Baimova, S. V. Dmitriev, K. Zhou, Thermal Conductivity of Silicene Nanosheets and The Effect of Isotopic Doping, Journal of Physics D: Applied Physics, Vol. 47, No. 16, 2014, pp. 165301, https://doi.org/10.1088/0022-3727/47/16/165301.

[25] R. Zhu, E. Pan, P. W. Chung, X. Cai, K. M. Liew, A. Buldum, Atomistic Calculation of Elastic Moduli in Strained Silicon, Semiconductor Science and Technology, Vol. 21, No. 7, 2006, pp. 906-911, https://doi.org/10.1088/0268-1242/21/7/014.

[26] C. Kittel, Introduction to Solid State Physics, 8th Edition, Wiley, New York, 2004.

[27] Z. Hashin, S. Shtrikman, A Variational Approach to the Theory of The Elastic Behaviour of Polycrystals, ournal of the Mechanics and Physics of Solids, Vol. 10, No. 4, 1962, pp. 343-352, https://doi.org/10.1016/0022-5096(62)90005-4.